PERGAMON

Modeling of radiation transfer and emission spectra in laser-induced plasma of Al vapor

V.I. Mazhukin[a], V.V. Nossov[a], G. Flamant[b, *], I. Smurov[c]

[a]*Institute of Mathematical Modelling RAS, 125047, Miusskaya 4a, Moscow, Russia*
[b]*Institut de Science et de Génie des Matériaux et Procédés CNRS, BP 5 Odeillo
66125 Font-Romeu Cedex, France*
[c]*Ecole Nationale d'Ingénieurs de Saint-Etienne, 58 rue Jean Parot, F-42023 Saint-Etienne Cedex 2, France*

Abstract

The influence of radiation transfer on dynamics of laser-induced plasma of Al vapor is analyzed numerically. Mathematical description of the plasma is performed in the framework of the transient 2D radiation gas dynamics (RGD); the multi-group diffusion approximation with 7–1000 spectral intervals is used to describe plasma radiation transfer. The performed research allows us to conclude that radiative transfer substantially affects the expansion of laser plasma for the nanosecond action intensity of 10^9–2×10^{10} W/cm^2 and the pulse energies of 0.02–0.4 J. The radiative energy losses can reach 60% of the laser pulse energy absorbed by the plasma. The spectral composition of escaping radiation is non-equilibrium and qualitatively corresponds to the optically thin approximation. The application of the Planck averaging technique make it possible to predict the correct values of total quantities (integrated over the entire frequency spectrum) using several tens of groups. © 2002 Elsevier Science Ltd. All rights reserved.

Keywords: Laser plasma; Radiation transfer; Emission spectra

1. Introduction

Analysis of radiation transfer is one of the most interesting and complex problems in the field of plasma investigation. As shown in Ref. [1], if the plasma temperature does not exceed several tens of electron-volts and its density is not too low, the energy and pressure of plasma radiation are much smaller as compared to the energy and pressure of the matter. The influence of radiation can manifest itself in radiative energy losses of the plasma and, in general, in redistribution of energy by radiative transfer.

---

* Corresponding author. Tel.: +33-4-68-30-7758; fax: +33-4-68-30-2940.
E-mail address: flamant@imp.cnrs.fr (G. Flamant).

Among a great number of studies devoted to laser ablation and laser plasma, there are only a few where the main attention is paid to the analysis of the radiation transfer contribution. In particular, it has been found [2,3] that microsecond laser radiation with the intensity of 5–50 MW/cm^2 causes 5–10% of the energy absorbed in the plasma to be removed. In Ref. [4] it has been established that under the action of the nanosecond eximer laser on the Al target with the radiation intensity of 10^9 W/cm^2 the radiative energy losses of the plasma are as high as 35%. On the other hand, it has been shown in Ref. [5], devoted to investigation of the structure of the eximer laser induced plasma that the plasma expansion is spherical and after the pulse termination is well described by the Sedov theory of instantaneous explosion that does not take radiative losses into account.

For the analysis of radiation transfer the properties of medium are described by the absorption coefficient that is characterized by complex dependence on radiation frequency [1,6]. The most accurate determination of the coefficient should provide resolution of single lines (line-by-line approach). For the cases of the atomic plasma of wide temperature range [7] and molecular gases [8] the approach requires 10^4–10^6 spectral points. Therefore, various simplified models are usually applied in scientific and engineering computations [1,7–9] that predict correct values of total quantities (transmission, radiative heat flux, radiative energy losses) at much lower spectral resolution.

The main purpose of the present study is to determine the effect of radiative transfer on gas dynamics, radiative and spectral characteristics of Al vapor plasma induced by the action of Nd-YAG laser with the wavelength of 1.06 μm, the intensity of 10^9–2 × 10^{10} W/cm^2, and the pulse duration of 10 ns. Particular attention is paid to the effect of the radiation spectral composition on the phenomena under examination.

2. Mathematical model

The problem has the axial symmetry and is solved in the cylindrical coordinate system introduced in the domain above the target. The z-axis coincides with the laser beam axis and is directed along the normal to the target surface, the r-axis is directed along the surface. The plasma evolution is described by the complete system of equations for radiative gas dynamics (RGD) supplemented by the transfer equation for laser radiation and two equations of state [4,10]:

$$\frac{\partial \rho}{\partial t} + \frac{1}{r}\frac{\partial}{\partial r}(r\rho u) + \frac{\partial}{\partial z}(\rho v) = 0, \tag{1}$$

$$\frac{\partial(\rho u)}{\partial t} + \frac{1}{r}\frac{\partial}{\partial r}(r\rho u^2) + \frac{\partial}{\partial z}(\rho uv) = -\frac{\partial(p+\omega)}{\partial r}, \tag{2}$$

$$\frac{\partial(\rho v)}{\partial t} + \frac{1}{r}\frac{\partial}{\partial r}(r\rho uv) + \frac{\partial}{\partial z}(\rho v^2) = -\frac{\partial(p+\omega)}{\partial z}, \tag{3}$$

$$\frac{\partial(\rho e)}{\partial t} + \frac{1}{r}\frac{\partial}{\partial r}(r\rho ue) + \frac{\partial}{\partial z}(\rho ve) = -p\left[\frac{1}{r}\frac{\partial(ru)}{\partial r} + \frac{\partial v}{\partial z}\right] - \left[\frac{1}{r}\frac{\partial q_r}{\partial r} + \frac{\partial q_z}{\partial z}\right] + \left[\frac{\partial G}{\partial z}\right], \tag{4}$$

$$\vec{\Omega}\,\mathrm{grad}\,I_v + \kappa_v I_v = \kappa_v I_{bv}, \quad \vec{q} = \int_0^\infty \partial v \int_{-1}^1 I_v \mu \partial \mu, \tag{5}$$

$$\frac{\partial G}{\partial z} - \kappa G = 0, \tag{6}$$

$$p = p(\rho, T), \tag{7}$$

$$e = e(\rho, T), \quad 0 < (r \times z) < (L_r \times L_z), \quad 0 < t < t_{max}. \tag{8}$$

Here ω denotes the artificial viscosity; q_r, q_z are the components of the total radiative heat flux, G denotes the laser radiation intensity; $\vec{\Omega}$ is the unit vector of direction of the photon; I_v, I_{bv} are the spectral intensity of the radiation and the blackbody radiation; κ_v, κ denote the absorption co-efficients for the thermal radiation and the laser radiation, respectively. The system of equations is supplemented by the initial and boundary conditions [4,10]. To estimate the parameters of the initial plasma layer the model of target heating, melting and evaporation is used developed by the authors [11].

The absorption coefficients κ_v, κ are determined by the Hartree–Fock–Slater quantum-mechanical model [7]. The total absorption coefficient is written as $\kappa_v = \sum_i n_i \sigma_i^{bf}(v) + \sum_{jk} n_j \sigma_{jk}^{bb}(v) + \kappa_v^{ff}$, where n_i, n_j denote the population of the excited states of atoms and ions, κ_v^{ff} is the Inverse Bremsstrahlung absorption coefficient, $\sigma_i^{bf}, \sigma_{jk}^{bb}$ are the absorption cross-sections for the bond–free and bond–bond transitions. Summation is performed for all the permitted transitions included into the model. The cross-section for the bond–bond transition is determined as the product of the oscillator strength and the spectral function of the line, the latter being calculated with account for several line broadening mechanisms. Calculation of the ionization balance and the charge states is performed within the collisional radiative model (CRM). The multi-group diffusion approximation is applied to describe the radiation transfer of the plasma [1,6]. In the framework of the method κ_v is assumed to be independent of frequency within the specified spectral sub-intervals (groups), and is substituted by the Planck mean absorption coefficient: $\kappa_{\Delta v} = \int_{\Delta v} \kappa_v U_{bv} \, dv / \int_{\Delta v} U_{bv} \, dv$, where U_{bv} means the energy density of blackbody radiation.

3. Results and analysis

3.1. Computation parameters and initial conditions

The influence of radiative transfer on expansion of the laser-induced plasma of Al vapor is analyzed in the following range of the laser parameters: the peak intensity $G_0 = 10^9$–2×10^{10} W/cm^2, the pulse duration $\tau = 10$ ns, the laser wavelength $\lambda = 1.06$ μm, and the focal spot radius $R = 0.025$ cm. The laser pulse intensity is considered to be uniformly distributed in space and time, $G \equiv G_0$. The chosen parameters correspond to the fluency of 10–200 J/cm^2 and the pulse energy of 0.02–0.4 J. The initial parameters of the plasma layer $0 \leqslant (r \times z) \leqslant (r_{hot} \times z_{hot})$, $T(0, r, z) = T_{hot}$, $\rho(0, r, z) = \rho_{hot}$ are chosen as follows: $z_{hot} = 20$ μm, $T_{hot} = 0.5$ eV, $\rho_{hot} = 5 \times 10^{-2}$ cm^{-3}, $r_{hot} = R$. The sizes L_r, L_z of the computational domain are $L_r = 5$ cm, $L_z = 25$ cm, the background temperature and the density are $T_0 = 0.03$ eV, $\rho_0 = 3 \times 10^{-6}$ g/cm^{-3}, respectively, which corresponds to the background pressure of $\approx 2 \times 10^{-3}$ bar. In all the computations the radiative transfer is considered in the spectral range of 0.1–200 eV that is divided into sub-intervals as follows: 0.1–1 eV is covered by one interval, while

the logarithmically-equidistant grid is applied in the range of 1.0–200 eV. The results presented in the paper refer to the total number of groups 7, 21, 61, 101 and 1001.

3.2. Description of plasma expansion

The temperature distributions predicted for $G_0 = 10^9$, 5×10^9, 2×10^{10} W/cm^2 are shown in Figs. 1 and 2. Fig. 1 corresponds to the time $t = 10$ ns. The distributions at all the intensities are characterized by the presence of a hot region (the plasma core) at the temperature of about 10, 15 and 20 eV. The major part of the plasma pattern has a lower temperature, while a sharp decrease of the temperature is observed at the pattern boundaries. The variation of the pattern shape with the intensity can also be seen in the figures. At 10^9 W/cm^2 the expansion in axial and radial directions proceeds at almost the same speed and the shape of the pattern is circular. As the intensity increases the axial expansion becomes more pronounced and at 2×10^{10} W/cm^2 the axial size is twice as long as the radial one. In all the three cases the expansion proceeds in Laser Supported Detonation (LSD) [12] regime at a typical speed of axial expansion in the range of 40 km/s at 10^9 W/cm^2 to 150 km/s at 2×10^{10} W/cm^2. For the later instant of time, Fig. 2, the plasma temperature decreases 2–3 times. At this stage the pattern shape is similar for the three cases and is characterized by the axial and radial sizes in the ratio of 2:1.

The results in Fig. 3 makes it possible to describe the effect of radiative transfer on the plasma temperature dependencies. The $T(r = 0, z)$ the temperature cross-sections along the beam axis, are presented at the time 10 ns for computations with different numbers of spectral groups. Exclusion of radiative transfer leads to strongly overestimated values of temperature. The maximum deviation of 20 eV or $\approx 50\%$ is at 2×10^{10} W/cm^2. At the intensity of 10^9 W/cm^2 the accurate temperature distribution is obtained with just 7 spectral groups. For the effect of higher intensity the convergence with respect to the group number is reached using 61–101 groups.

3.3. Plasma radiative energy losses

Consider in detail the evolution of the part of energy removed by the radiation through each of the surfaces (Fig. 4). The major part of energy is removed during the laser action and over a short period after the pulse termination. The side boundary energy removal is twice as high as the one of the upper boundary, in spite of the fact the frontal radiative flux has approximately twice higher intensity. It becomes clear, however, if one compares the areas of the two boundary surfaces that are $\pi \Delta R^2(t)$ for upper boundary and $2\pi \Delta R(t) \Delta Z(t)$ for the side one ($\Delta R(t), \Delta Z(t)$) being the radial and axial sizes of the plasma pattern) and takes into account that $\Delta Z(t) \approx 2\Delta R(t)$ (Fig. 2) is typical of the regimes under consideration. Energy removal toward the target does not exceed 1%.

Computations of the total part of the energy removed by the radiation $E_{emitted}/E_{laser}$ with different numbers of spectral groups (Fig. 5) show that the spectral accuracy plays an important role in analysis of plasma radiative characteristics. The radiative losses increase with the increase of the laser intensity: from $\approx 10\%$ at $G_0 = 10^9$ W/cm^2 to $\approx 60\%$ at $G_0 = 2 \times 10^{10}$ W/cm^2. The application of the small number of groups result in overestimation of the radiative energy removal. The maximum difference between the values of $E_{emitted}/E_{laser}$ ratio predicted with 7 and 101 groups is $\approx 25\%$ and is reached at the lowest laser intensity. For all the laser action regimes the results with 61 and 101 groups are in good agreement.
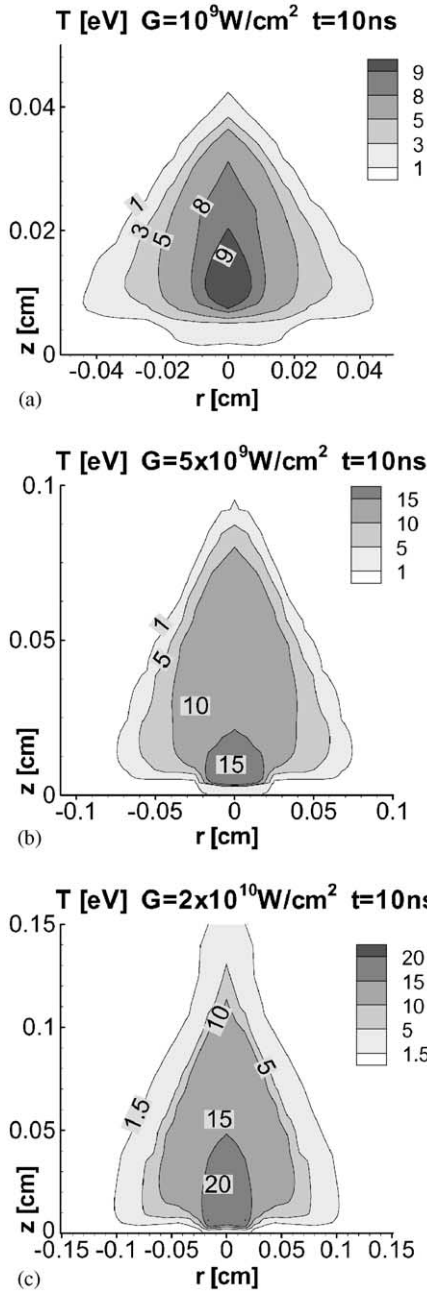
Fig. 1. Plasma temperature distributions at the laser intensity $G_0 = 10^9$, 5×10^9, 2×10^{10} W/cm^2 at the time instant of 10 ns.
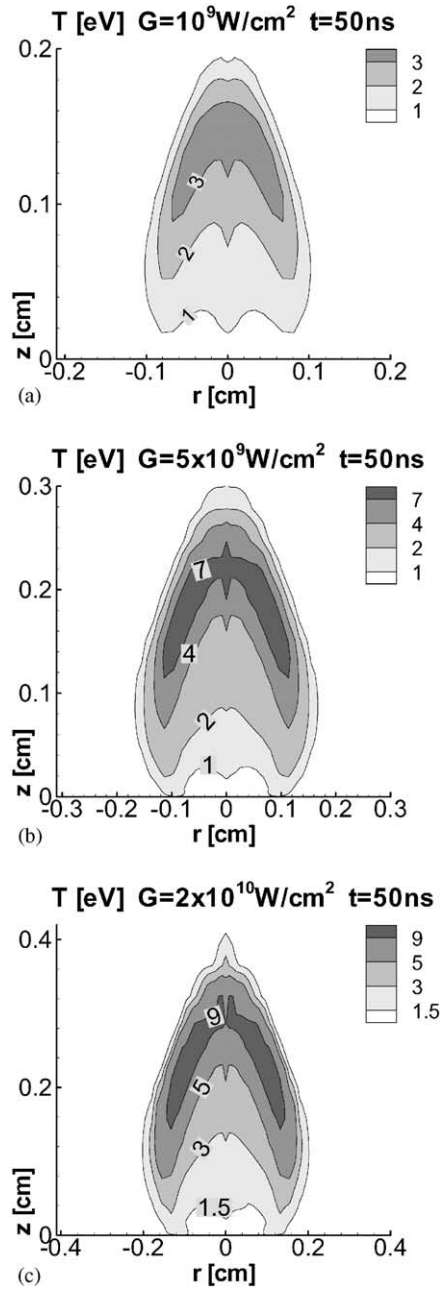
Fig. 2. Plasma temperature distributions at the laser intensity $G_0 = 10^9$, 5×10^9, 2×10^{10} W/cm^2 at the time instant of 50 ns.
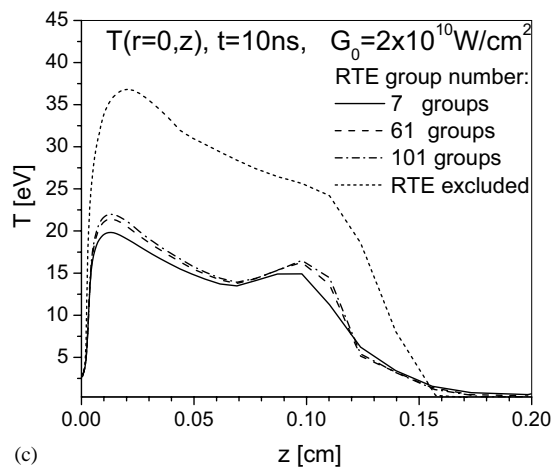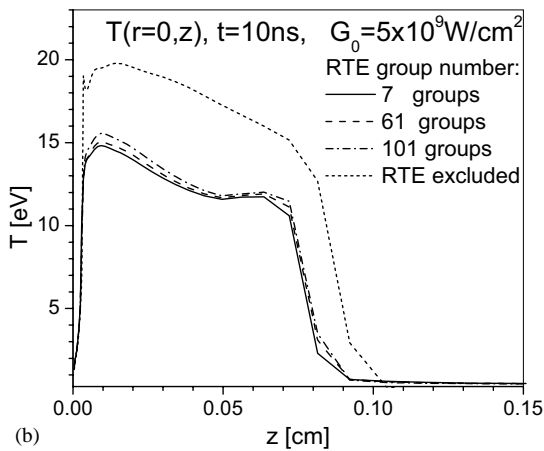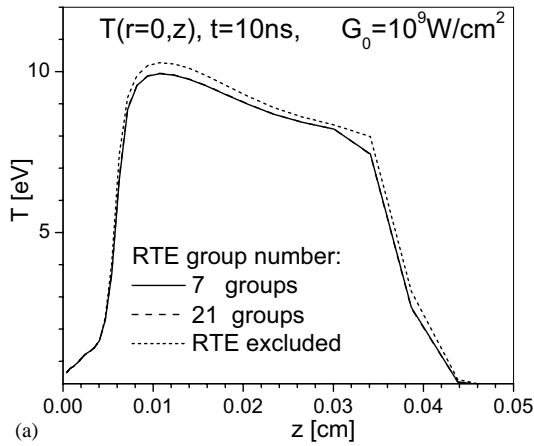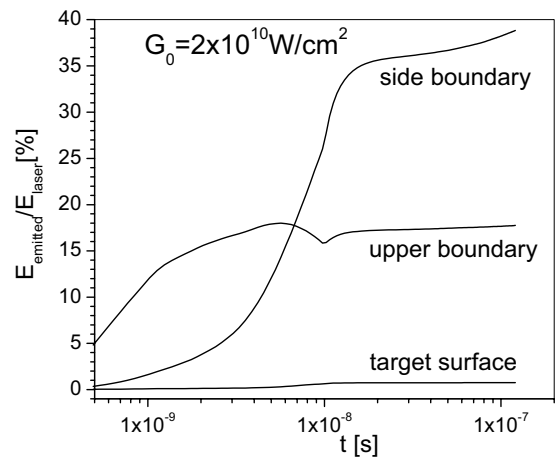
Fig. 3. Plasma temperature profiles at the beam axis at the laser intensity $G_0 = 10^9$, 5×10^9, 2×10^{10} W/cm^2 at the time instant of 10 ns.
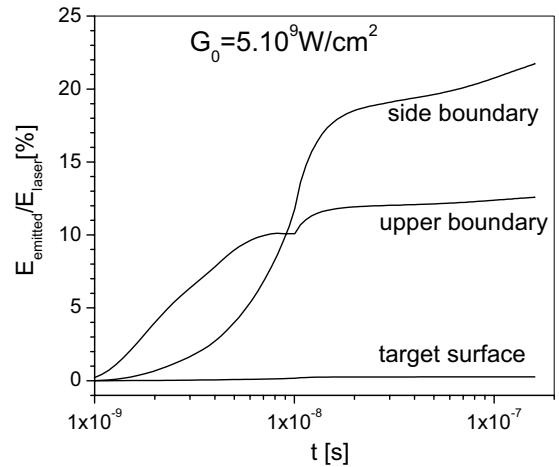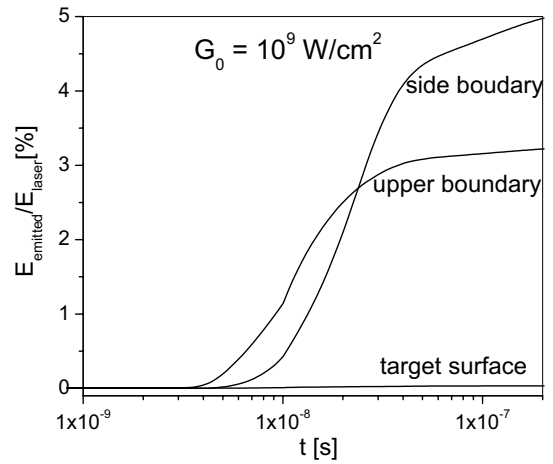
Fig. 4. Radiative energy removal through the upper boundary, side boundary, and the target surface at the laser intensity $G_0 = 10^9$, 5×10^9, 2×10^{10} W/cm^2.
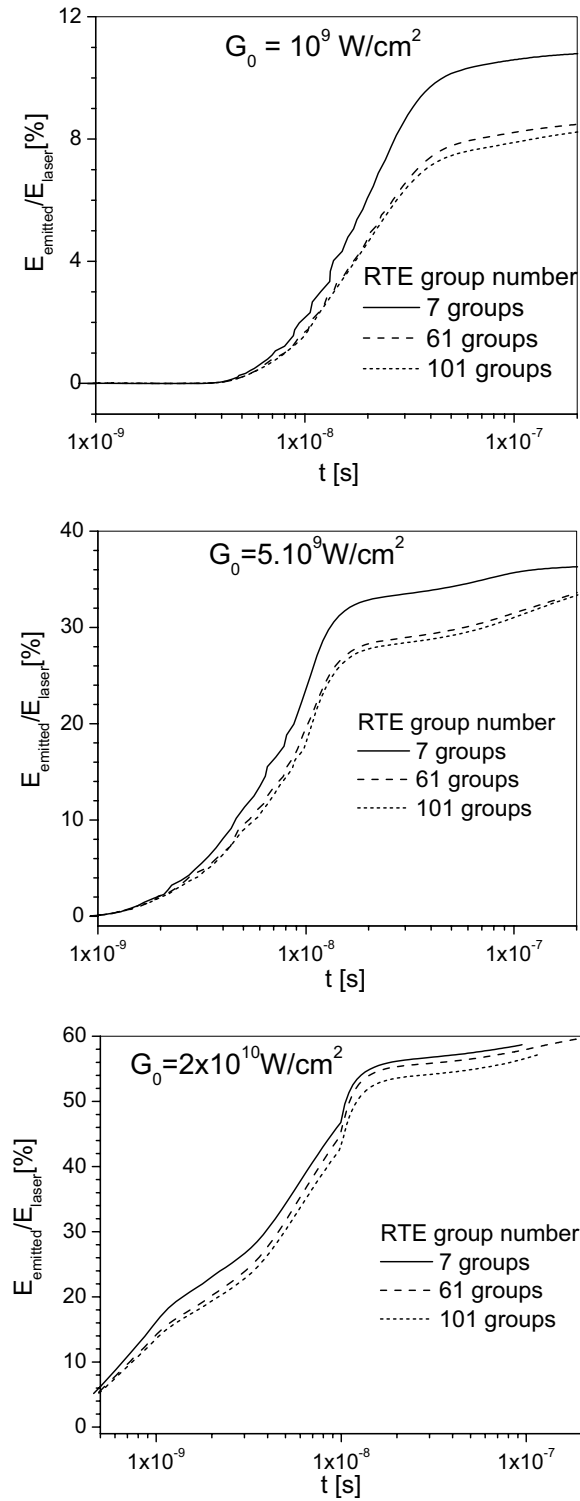
Fig. 5. Total radiative energy removal at the laser intensity $G_0 = 10^9$, 5×10^9, 2×10^{10} W/cm^2.
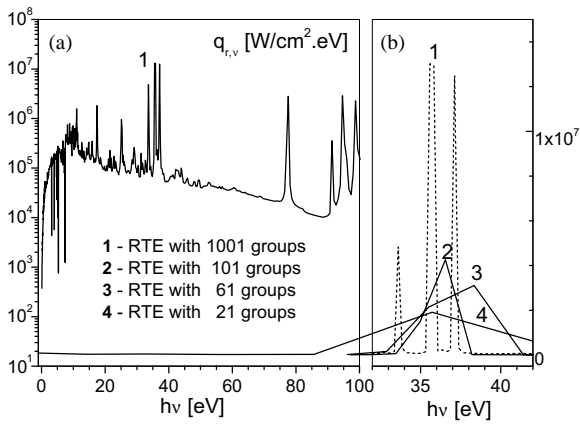
Fig. 6. Spectral radiative heat flux at the side boundary at $t = 10$ ns for the laser intensity $G_0 = 5 \times 10^9$ W/cm^2.
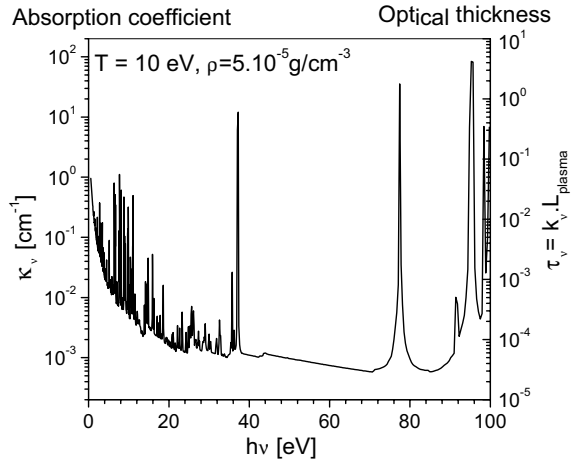
Fig. 7. Absorption coefficient and optical thickness of the plasma at $T = 10$ eV, $\rho = 5 \times 10^{-5}$ g/cm^3, $L_{plasma} = 0.15$ cm.

3.4. Spectral characteristics of plasma

Spectral dependencies of the side radiative flux $q_{r,v}$ at the time $t = 10$ ns determined with the laser intensity of $G_0 = 5 \times 10^9$ W/cm^2 and the different number of spectral groups are shown in Fig. 6. The most pronounced feature of the spectra is their non-equilibrium with a number of strong lines that can be reproduced by only the most detailed spectral grid (Fig. 6a). The plots for the narrower spectral range (Fig. 6b) show that as the number of the groups decreases (curves 2, 3, 4) the lines become indistinguishable, and the intensity of the escaping radiation decreases inversely proportionally to the width of respective spectral interval.

The optical characteristics of the plasma are illustrated in Figs. 7 and 8. The absorption coefficient and the optical thickness ($\tau_v = \kappa_v L_{plasma}$) are presented for the typical values of the temperature, density and size of the plasma cloud (Fig. 7). The solid line in Fig. 8 corresponds to the optically thin approximation of the radiative flux $q_v = c/2 \times \tau_v U_{bv}$ [1] and the dashed one is the blackbody radiation intensity. As seen the plasma is optically thin ($\tau_v \ll 1$) for the most parts of the spectrum, and, as a consequence, the optically thin approximation qualitatively corresponds to the computed spectrum (Fig. 6a). Under these conditions the application of the Planck averaging technique allows one to accurately determine the total quantities with the small number of spectral groups. At the same time the optically thin condition is not fulfilled for the strongest lines and the optically thin approximation that does not account for reabsorption process predicts physically meaningless values higher than the blackbody radiation intensity.

In real plasma spectroscopy, observations are usually performed in a narrow spectral region lying in either visible or UV part of the spectrum 2–5 eV. The spectral gap is adjusted to the strongest lines of the matter, that, in case of Al, are AlI 3.14 eV and AlI 4.02 eV. These lines correspond to transition from the first $4^2S_{1/2}$ and second $3^2D_{3/2,5/2}$ excited levels of neutral Al to the ground state $3^2P_{1/2,3/2}$. The predicted spectrum for the effect of $G_0 = 5 \times 10^9$ W/cm^2 is shown in Fig. 9. The computation has been performed on the spectral grid with 60 nodes distributed over the whole range
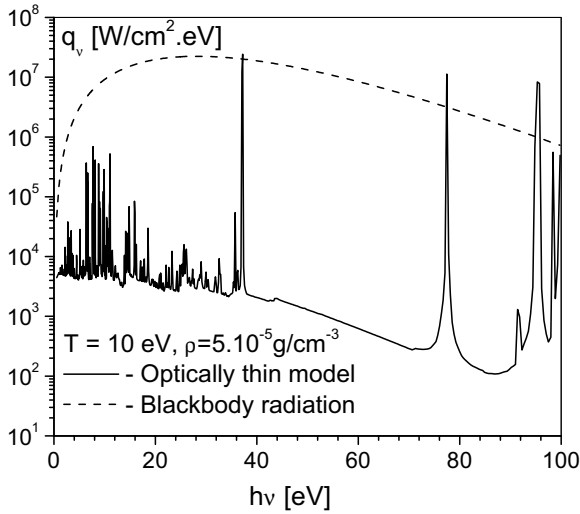
Fig. 8. Spectral radiative heat flux approximations by the optically thin model and Planck function (blackbody radiation).
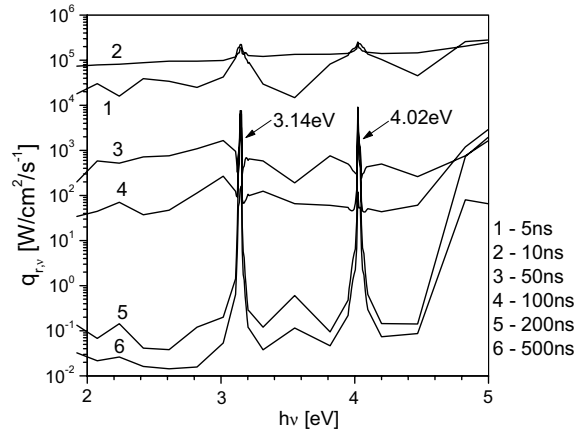
Fig. 9. Evolution of spectral lines AlI 3.14 eV and AlI 4.02 eV of radiative heat flux at side boundary for the laser intensity $G_0 = 5 \times 10^9$ W/cm^2.

plus 16 points distributed equidistantly in the each of 3.0–3.2 and 3.9–4.1 eV sub-ranges (vicinities of the lines). Thus the spectral resolution in these intervals was 0.0125 eV. During the pulse (Fig. 9, curves 1 and 2) the lines are not practically seen or are strongly broadened. Starting from the time $t = 50$ ns, the lines become visible and the ratio of peak to background intensity increases in the course of time. Besides for the later period the lines broaden, (curves 5, 6), however, the spectral resolution appears to be insufficient to accurately follow this effect.

4. Conclusion

The performed study allows us to conclude that radiative transfer substantially affects the expansion of laser plasma for the intensity of 10^9–2×10^{10} W/cm^2 and pulse energies of 0.02–0.4 J.

- The radiative energy losses can reach 60% of the laser pulse energy absorbed by the plasma and lead to a proportional decrease of the temperature. Radiative energy is removed mainly in the frontal and side directions.
- The spectral composition of escaping radiation is non-equilibrium and qualitatively corresponds to the optically thin approximation. The application of the Planck averaging technique allows one to predict the correct values of total quantities (integrated over the entire frequency spectrum) using several tens of groups.
- By using the detailed frequency grid for the selected spectral intervals the model makes it possible to observe evolution of the spectral lines.

References

[1] Zeldovich YaB, Raizer YuP. Physics of shock waves and high temperature hydrodynamics phenomena I. New York: Academic Press, 1967.

[2] Mazhukin VI, Smurov I, Flamant G. Simulation of laser plasma dynamics: influence of ambient pressure and intensity of laser radiation. J Computational Phys 1994;112:78–90.

[3] Elyashevich MA, Minko LYa, Romanov GS, Stankevich YuA, Chivel YuA, Chumakov AN. Dinamika plasmi, voznikajuchej pri vozdejstvii lasernogo izluchenija na tverdotelnije pregradi. Docl Acad Nauk SSSR—Phys Ser 1985;49:1132–5.

[4] Ho JR, Grogoropoulos CP, Humphrey JAC. Gas dynamics and radiation heat transfer in the vapor plume produced by pulsed laser irradiation of Al. J Appl Phys 1996;79:7205–15.

[5] Schittenchelm H, Callies G, Berger P, Hugel H. Investigations of extinction coefficients during excimer laser ablation and their interpretation in terms of Rayleigh scattering. J Phys D 1998;31:418–30.

[6] Modest M. Radiative heat transfer. New York: McGraw-Hill, 1993.

[7] Romanov GS, Stankevich YuA, Stankevich LK, Stepanov KL. Thermodynamic and optical properties of gases in a wide range of parameters. Int J Heat Mass Transfer 1995;38:545–56.

[8] Taine J, Soufiani A. Gas IR Radiative properties: From spectroscopic data to approximate models. J Adv Heat Transfer 1999;33:295–412.

[9] Goutiere V, Liu F, Charette A. An assessment of real gas modeling in 2D enclosures. JQSRT 2000;64:299–326.

[10] Chetveruskin BN. Dinamika izluchayushchego gaza of radiative gas. Moscow: Nauka, 1992.

[11] Mazhukin VI, Samarskii AA. Mathematical Modeling in the Technology of Laser Treatments of Materials. Surv Math Ind 1994;4:85–149.

[12] Raizer YuP. Physics of gas discharge. Moscow: Nauka, 1987.